Int. J. Multiphase Flow Vol. 8, No. 2, pp. 165–181, 1982
Printed in Great Britain.

03019322/82/020165–17$03.00/0
Pergamon/Elsevier

CHF OF FORCED CONVECTION BOILING IN UNIFORMLY HEATED VERTICAL TUBES: EXPERIMENTAL STUDY OF HP-REGIME BY THE USE OF REFRIGERANT 12

Y. KATTO and S. YOKOYA
Department of Mechanical Engineering, University of Tokyo, Hongo, Bunkyo-ku, Tokyo, Japan

Abstract—For the critical heat flux in HP-regime, that is high-pressure regime, almost no data having been published for fluids other than water, an experimental study is attempted on R-12 boiling in 5- and 3-mm dia. and 1000-mm long tubes. Critical heat flux q_c is measured in the range of pressure $p = 19.6$–34.3 bar (vapor-to-liquid density ratio $\rho_G/\rho_L = 0.109$–0.306), mass velocity $G = 1100$–$9000\ \mathrm{kg/m^2s}$, and inlet subcooling enthalpy $\Delta H_i = 0$–$65\ \mathrm{kJ/kg}$. Depending on the condition of G and ΔH_i, CHF takes place with natures which can be divided into two categories, regular and anomalous. For regular CHF, critical condition is detected first at the exit end of heated tube and a linear $q_c - \Delta H_i$ relationship holds, whereas anomalous CHF initiates its critical condition upstream of the tube exit and exhibits involved relationship between q_c and ΔH_i. Experimental data of regular CHF are found to agree fairly well with the predictions of two different generalized correlations proposed recently by Katto and by Shah respectively although some systematic differences proper to each correlation exist.

1. INTRODUCTION

Many experimental studies have been made on critical heat flux (CHF) of forced convection boiling in uniformly heated vertical tubes fed with subcooled water to clarify the fundamental natures of CHF in connection with their application in nuclear reactors. Compared with this, the studies on CHF of boiling water at high pressures and high mass velocities, as connected with steam generators or conventional steam boilers, are not necessarily numerous. Nevertheless, the pioneer studies of Peskov *et al.* (1969), Becker *et al.* (1972), and Campolunghi *et al.* (1974) (see table 1 for their experimental conditions of heated tube length l, tube diameter d, vapor-to-liquid density ratio ρ_G/ρ_L, and mass velocity G) have revealed that when the mass velocity is high, CHF at high pressures exhibits different characters from those observed at low to moderate pressures. In addition, empirical equations for predicting CHF of water at high pressures have been presented by Peskov *et al.* (1969), Lee (1970), and Becker *et al.* (1972) respectively, and these give very high accuracies. In the paper of Becker *et al.* (1972), the lower limit of the mass velocity to originate the high-pressure regime is also given as a function of pressure.

Meanwhile, for existing data of CHF obtained for different fluids in uniformly heated tubes, two generalized corrleations were recently proposed by Katto (1978, 1979, 1980a) through a formulation method and by Shah (1979) through a graphical method, including the above-mentioned high-pressure regime. The former correlation classifies CHF into four characteristic regimes called L, H, N and HP, where L-, H- and N-regime appear when the mass velocity is low, moderate and high respectively, while HP-regime is the regime which replaces N-regime when the system pressure is sufficiently high corresponding to the above-mentioned high-pressure regime. The latter correlation may be considered to give the high-pressure regime for reduced pressure $p_r \geqq 0.6$ although a special narrow transition region exists for $p_r = 0.3$ to 0.6. These two correlations are possibly inferior to Peskov, Lee and Becker correlations as regards the accuracy for predicting CHF of water at high pressures, but are in the generalized forms capable of predicting CHF of the fluids other than water. It must be noted, however, that almost all existing data of CHF obtained for very high ρ_G/ρ_L ratios are of water except for the restricted data of liquid helium obtained for low l/d ratios less than ~50 (see Katto 1979, 1980a). Namely, in addition to the above-mentioned water data of Peskov *et al.*, Becker *et al.* and Campolunghi *et al.*, there are water data belonging to the high-pressure regime obtained in the experiments of Chojnowski & Wilson (1974), Watson *et al.* (1974), Doroschuk *et al.* (1975) or Levitan & Lantzman (1975), and the old data compiled in tables 11–14 of Thompson &

Table 1. Main conditions of cited experiments for vertical tubes

Main Regime	Author	Fluid	l(cm)	d(cm)	l/d	ρ_v/ρ_l	G(kg/m^{2}s)	Remark
HP	Peskov et al.1969	Water	89.0-210	0.80	111-263	0.144-0.366	1110-5000	Slow and small temp. rise CHF*
	Becker et al.1972	Water	200-500	1.0	200-500	0.140-0.347	1000-7000	
	Campolunghi et al.1974	Water	~1100	1.2	~937	0.0902-0.176	1100-2600	
	Chojnowski-Wilson 1974	Water	762	3.2	238	0.243	682-1462	
	Watson et al.1974	Water	549	3.78	145	0.271	407-2034	Upstream CHF
	Doroschuk et al.1975		150	0.80	188	0.201-0.271	1500-3000	
	Levitan-Lantzman 1975	Water	150	0.80	188	0.201-0.271	1500-3000	
	Thompson-Macbeth 1964	Water	69.6	0.191	365	0.171-0.285	1940-3780	Data in Tables 11-14
Near HP	Waters et al.1964	Water	366	1.12	327	0.0493-0.0853	6690-9320	Upstream CHF for G = 6690-9320 kg/m^{2}s
	Matzner et al.1965	Water	244-488	1.02	240-480	0.0484	1340-9480	Upstream CHF for G = 6900-9300 kg/m^{2}s
	Merilo 1977	R-12	244-488	1.26	194-387	0.0487	950-6500	Upstream CHF for G = 5500-6500 kg/m^{2}s
	Merilo-Ahmad 1979	R-12	103-305	0.53	194-575	0.0487-0.0768	1600-8100	Upstream CHF for G = 8100 kg/m^{2}s
H and N	Groeneveld 1972, 1974	R-12	138	0.78	177	0.0498	1330-8100	Upstream CHF** and slow CHF
HP	Present study	R-12	100	0.30-0.50	200-333	0.109-0.306	1100-9000	

* in case of high pressure and small ΔH_i. ** for mixed inlet conditions with $G > 4050$ kg/m^{2}s.

Macbeth (1964) include some water data in the high-pressure regime (see table 1 for high values of ρ_G/ρ_L of these data). Hence, as far as the high-pressure regime is concerned, both Katto and Shah correlations, although generalized, are virtually based on the water data such as mentioned above, and their applicability to the fluids other than water has not necessarily been confirmed.

Now, figure 1 illustrates the criterion for the onset of CHF in HP-regime proposed in the generalized correlation of Katto (1980a), where ρ_G is the density of vapor, ρ_L the density of liquid, l the length of heated tube, d the I.D. of heated tube, σ the surface tension, and G the mass velocity. Outlines of the process to deduce figure 1 will be explained afterward in Section 4.1. Within the region on the r.h.s. of a heavy curve in figure 1, if the value of dimensionless group $\sigma\rho_L/G^2l$ is lower than the indicated value, then CHF in HP-regime takes place there. This region will be hereafter referred to as HP-possible-region. According to Katto (1980a), the experimental data listed in table 1 from the first to the eighth line satisfy the above-mentioned criterion for the onset of HP-regime, and hence they are listed together under a mark of HP.

In connection with HP-regime, also attention must be paid to the experimental studies on CHF of water or R-12 made by Waters *et al.* (1964), Matzner *et al.* (1965), Merilo (1977), and Merilo & Ahmad (1979) for vertical tubes under conditions from the vicinity of the boundary of the HP-possible-region to the neighboring region in figure 1 (see table 1 for the conditions of l/d and ρ_G/ρ_L adopted in the studies). These studies, carrying out the experiments up to very high mass velocities, reported the observation of the phenomenon of upstream CHF, that is, the initiation of CHF condition upstream of the exit end of heated tube, in the ranges of or at G noted in the far right column of table 1. In addition, Groeneveld (1972, 1974, 1979) reported the observation of upstream CHF for $G > 4050$ kg/m^{2}s in his experiment of R-12 made under conditions far from HP-regime (see table 1 for the conditions of l/d and ρ_G/ρ_L) and with mixed inlet conditions. In the experiment of Groeneveld, slow CHF was also observed at high mass velocities, instead of the usual CHF temperature excursion, while Peskov *et al.* (1969) reported the observation that the wall temperature excursion at the onset of CHF declined noticeably with increasing pressure and decreasing inlet subcooling.

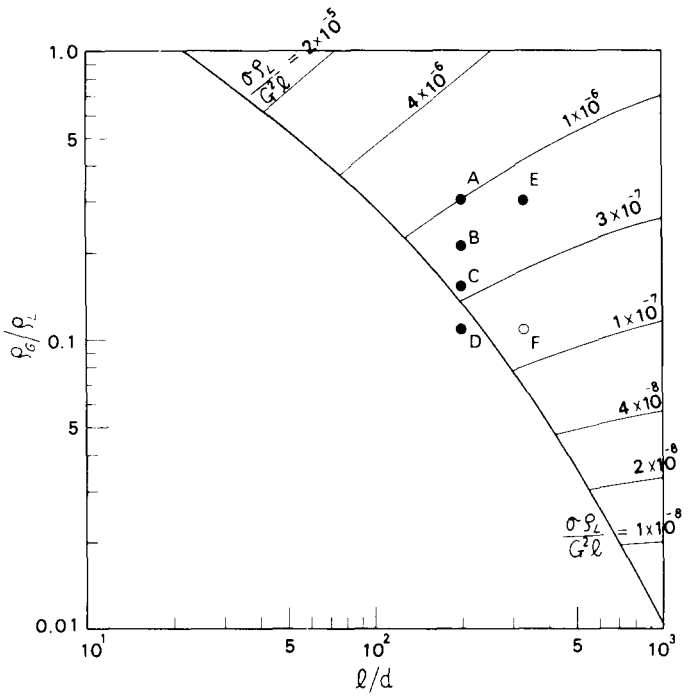

Figure 1. Criterion for the onset of CHF in HP-regime (Katto 1980a), and the experimental conditions adopted in this study.

In the present study, therefore, experiments are made for CHF in HP-regime employing R-12 as coolant (see the bottom line of table 1 for the experimental range) with three main purposes: (i) to provide CHF data of R-12 for HP-regime where most existing data are limited to those of water, (ii) to examine the two generalized correlations proposed recently by Katto and Shah on the generality of HP-regime correlation virtually based on water data alone, and (iii) to clarify the circumstances of generating anomalous phenomena such as upstream CHF, low temperature excursion and the like.

2. EXPERIMENTAL APPARATUS

The experimental apparatus employed is shown schematically in figure 2. Among the liquid of R-12 flowing out of a circulating pump, a part passes through flow meters and an electric preheater successively to enter the test section under subcooled conditions, and then the vapor/liquid two-phase flow leaving the test section flows into a pressurizer, that is a 200-mm dia. and 650-mm high vessel. Meantime, the rest of the liquid flowing out of the circulating pump passes through a cooler (4-pass concentric tube, counter flow heat exchanger cooled by water), and then the greater part of it returns to the circulating pump through a filter, while the rest is sprayed into the pressurizer to condense the vapor coming from the test section. The pressurizer, equipped with a water-cooled condenser and an electric heater in it, adjusts the temperature of saturated liquid in the vessel, and thereby the system pressure is kept at a prescribed value. Finally, the liquid flowing out of the pressurizer joins the subcooled liquid coming from the cooler to return to the circulating pump.

The test section, a stainless steel tube of I.D. $d = 5$ mm and 3 mm with wall thickness of 1 mm for both cases and length of heated section $l = 1000$ mm, is heated by direct passage of a d.c. current. As shown in figure 3, eleven 0.1-mm dia. Chromel–Alumel thermocouples are spot-welded to the outer wall of the heated section, and the temperature of these thermocouples are measured during the experiment. Besides, a CHF-detector is set to operate automatically

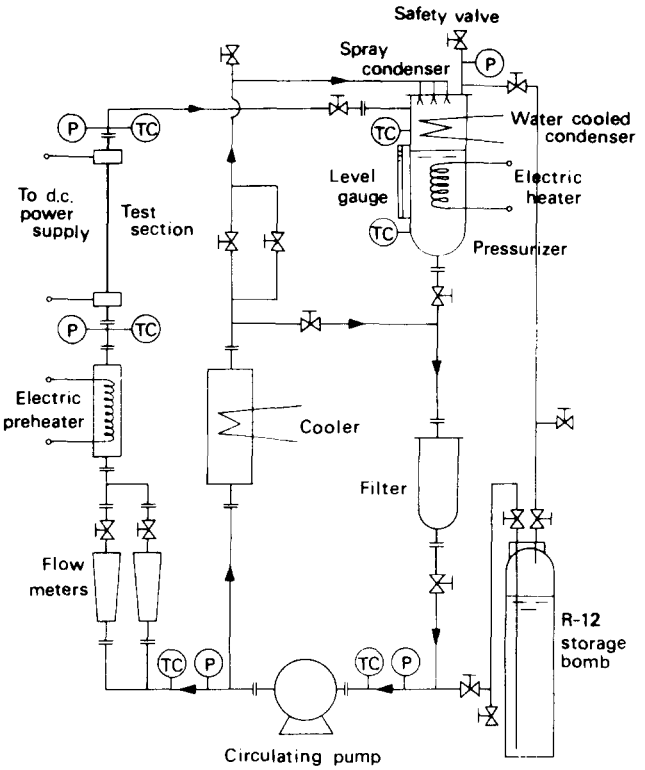

Figure 2. Experimental apparatus (P: pressure gauge, and TC: thermocouple).

for shutting off the d.c. current when the thermocouple TC1 near the exit end of heated section detects the wall temperature rise of 60°C higher than the saturation temperature. In case of upstream CHF, the d.c. current is shut off manually.

3. EXPERIMENTAL RESULTS

Experimental results obtained will be presented with the aid of figures to save the space (the tabulated data are obtainable from the authors if necessary).

3.1 *Data for 5-mm dia. tube*

For the heated tube of $d = 5$ mm and $l = 1000$ mm, experiments are made at pressures $p = 34.3$, 29.4, 24.5 and 19.6 bar, which correspond to the points A, B, C and D in figure 1 respectively. The results are presented in figure 4, which shows the variation of critical heat flux q_c with inlet subcooling enthalpy ΔH_i for fixed inlet pressure p and mass velocity G.

In figure 4, open circles represent the data of CHF detected by the thermocouple TC1 near the exit end of heated tube, while solid circles represent upstream CHF. The number of thermocouple (see figure 3), with which critical condition is detected first, is indicated by the side of solid circular data point partly for $p = 34.3$ and 19.6 bar alone to avoid complexity, showing the trend that (i) the range of ΔH_i to originate upstream CHF becomes wider with increasing p and G, and (ii) the location initiating critical condition moves gradually toward the inlet end of heated tube with decreasing ΔH_i. The broken curves in figure 4 have been drawn to indicate the boundary of the region of linear $q_c - \Delta H_i$ relationship, and it is noted that upstream CHF appears in the region on the l.h.s. of the broken curve.

For the upstream CHF shown in figure 4, the wall temperature rise at the onset of CHF is observed to be lower than that of the regular CHF detected by the CHF detector. In addition, even for the data of regular CHF at $G = 1100$ to 3300 kg/m^{2}s in figure 4, the trend of the reduction of CHF temperature excursion is observed under the conditions of $\Delta H_i \fallingdotseq 0$. These

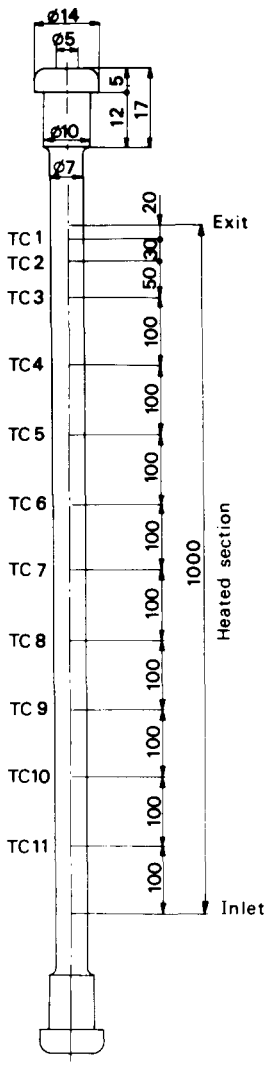

Figure 3. Test tube in case of $d = 5$ mm and the positions of thermocouples (unit of length: mm).

circumstances of wall temperature rise observed at the onset of CHF may be regarded as similar to the observation of Peskov *et al.* (1969).

Figure 5 shows the ratio of the pressure drop $-\Delta p$ through the test tube to the inlet pressure p, observed just before the onset of CHF.

3.2 *Data for 3-mm dia. tube*

For the heated tube of $d = 3$ mm and $l = 1000$ mm, experimental results of both q_c and $-\Delta p$ obtained at $p = 34.3$ bar (point E in figure 1) are shown in figure 6. Experiments were also made at $p = 19.6$ bar (point F in figure 1) with qualitatively similar results to figure 6, but the pressure drop through the test tube was extremely high so that the presentation of the data is omitted here.

For the heated tube of a diameter as small as 3 mm, upstream CHF does not take place within the experimental range, but a somewhat anomalous character for $q_c - \Delta H_i$ relationship is observed in the region on the l.h.s. of the broken curve in the top diagram of figure 6.

In the case of $d = 3$ mm, it is also observed that for the greater part of data shown in figure 6, the wall temperature rise at the onset of CHF is lower than that measured for the regular CHF in 5-mm dia. tube. However, this phenomenon may probably be due to the effect of heat

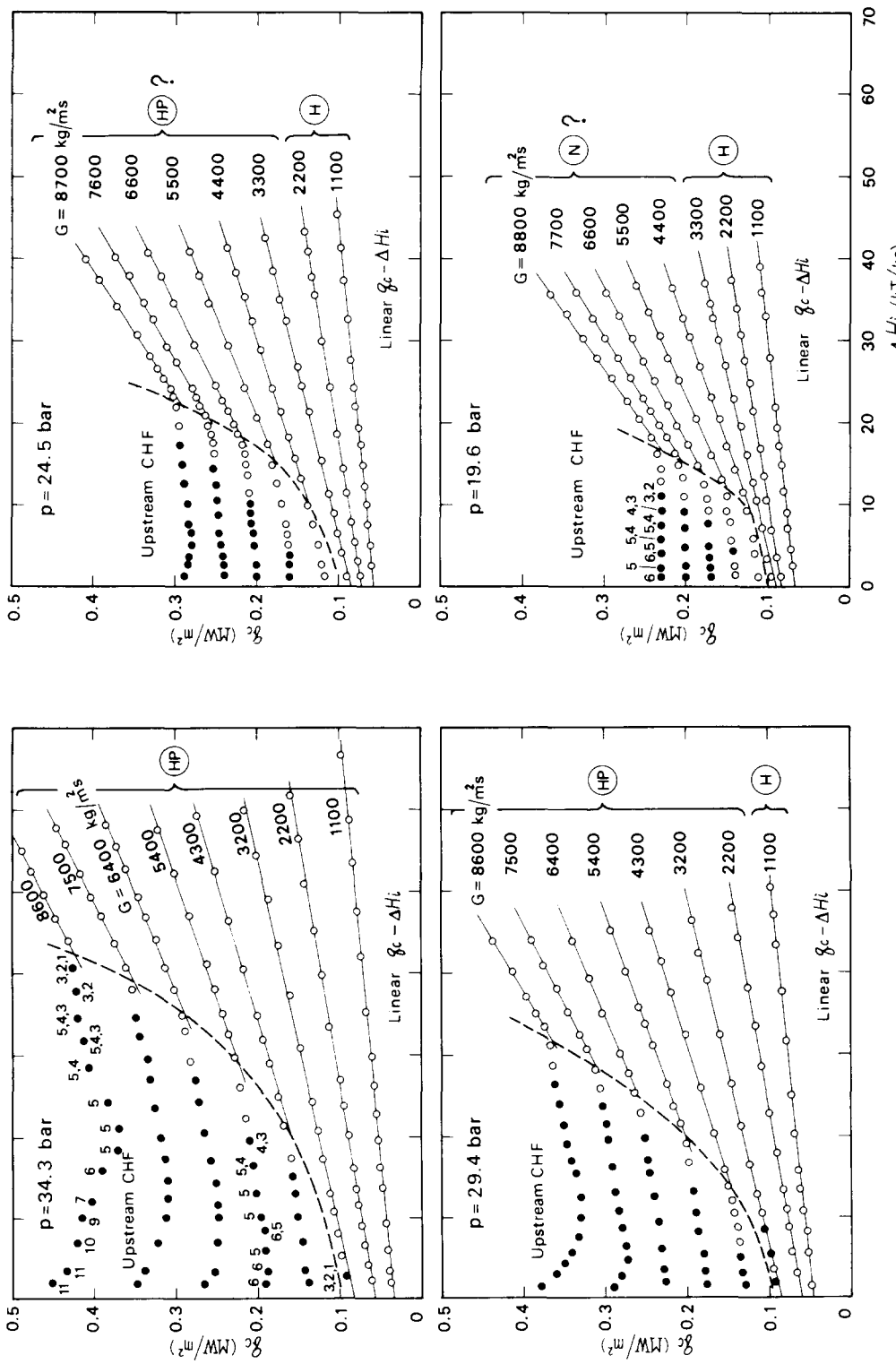

Figure 4. Experimental results of critical heat flux q_c for R-12, d = 5 mm, and l = 1000 mm (p = 34.3, 29.4, 24.5 and 19.6 bar correspond to points A, B, C and D in figure 1).

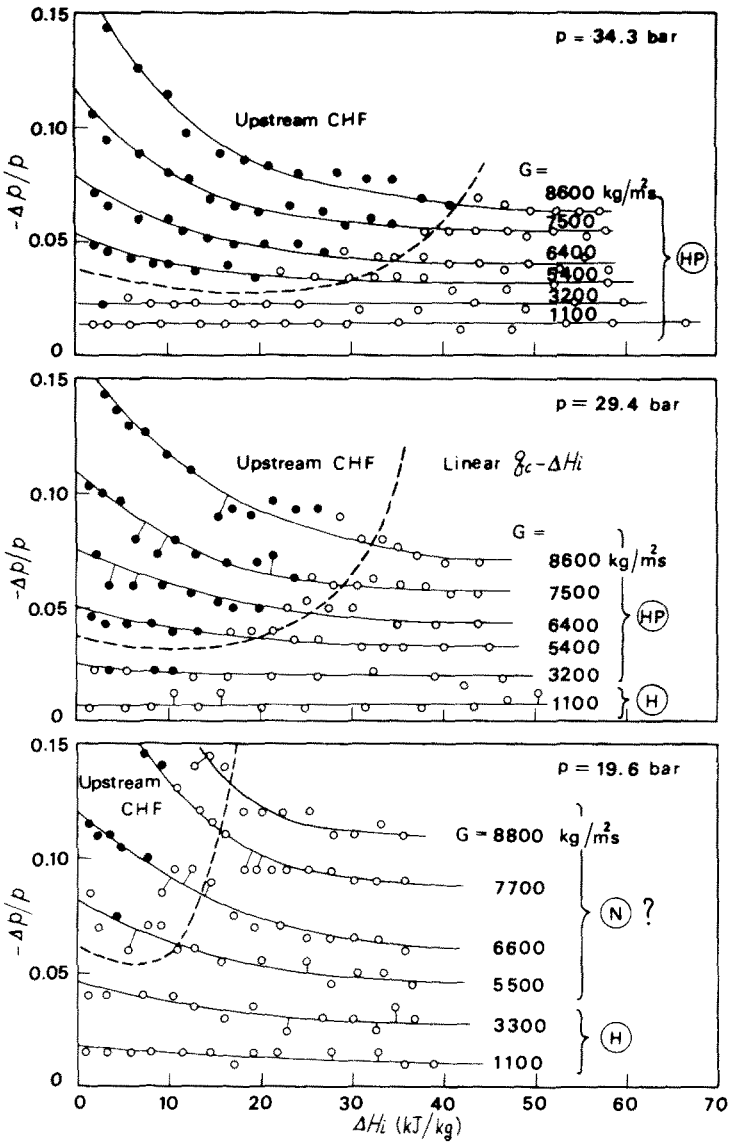

Figure 5. Pressure drop $-\Delta p$ through test tube just before the onset of CHF for R-12, $d = 5$ mm, and $l = 1000$ mm.

conduction through the tube wall at the exit end of heated section, because the wall thickness of 1 mm is considerable as compared with the tube diameter of 3 mm.

4. ANALYSIS OF DATA

4.1 *Preparation*

From the generalized correlation equations of CHF proposed by Katto (1980a), equations necessary in this chapter will be abstracted below, writing critical heat flux q_c for inlet subcooling enthalpy ΔH_i as:

$$q_c = q_{co}\left(1 + K\frac{\Delta H_i}{H_{LG}}\right) \qquad [1]$$

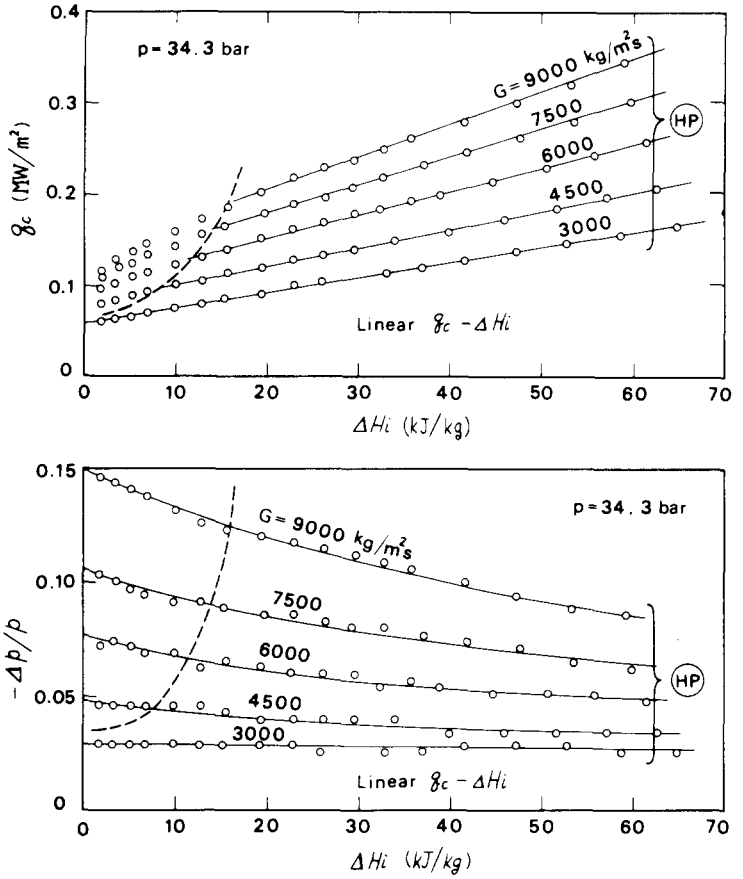

Figure 6. Experimental results of q_c and $-\Delta p$ for R-12, $d = 3$ mm, and $l = 1000$ mm ($p = 34.3$ bar corresponds to point E in figure 1).

where H_{LG} is the latent heat of evaporation. First, for q_{co} on the r.h.s. of [1], H- and N-regime:

$$\frac{p_{co}}{GH_{LG}} = 0.10\left(\frac{\rho_G}{\rho_L}\right)^{0.133}\left(\frac{\sigma\rho_L}{G^2 l}\right)^{1/3}\frac{1}{1+0.0031\,l/d} \qquad [2]$$

$$\frac{q_{co}}{GH_{LG}} = 0.098\left(\frac{\rho_G}{\rho_L}\right)^{0.133}\left(\frac{\sigma\rho_L}{G^2 l}\right)^{0.433}\frac{(l/d)^{0.27}}{1+0.0031\,l/d} \qquad [3]$$

HP-regime:

$$\frac{q_{co}}{GH_{LG}} = 0.0384\left(\frac{\rho_G}{\rho_L}\right)^{0.60}\left(\frac{\sigma\rho_L}{G^2 l}\right)^{0.173}\frac{1}{1+0.280(\sigma\rho_L/G^2 l)^{0.233}\,l/d}\,. \qquad [4]$$

Next, for K on the r.h.s. of [1],

K corresponding to q_{co} of [2]:

$$K = \frac{5}{6}\frac{0.0124 + d/l}{(\rho_G/\rho_L)^{0.133}(\sigma\rho_L/G^2 l)^{1/3}}. \qquad [5]$$

K to q_{co} of [3]:

$$K = 0.416\frac{(0.0221 + d/l)(d/l)^{0.27}}{(\rho_G/\rho_L)^{0.133}(\sigma\rho_L/G^2 l)^{0.433}}. \qquad [6]$$

K to q_{co} of [4]:

$$K = 1.12\frac{1.52(\sigma\rho_L/G^2l)^{0.233} + d/l}{(\rho_G/\rho_L)^{0.60}(\sigma\rho_L/G^2l)^{0.173}}. \quad [7]$$

Boundary between H- and N-regime relating to [3] is given by

$$\frac{\sigma\rho_L}{G^2l} = \left(\frac{0.77}{l/d}\right)^{2.70}. \quad [8]$$

Figure 7 illustrates the mutual relations between equations of [2] to [4] and [8] for fixed ρ_G/ρ_L and l/d. The prediction line of [2] intersects that of [3] at an open circle point, while two prediction lines of [2] and [4] intersect at a solid circle point P. For a given value of l/d, [8] fixes the horizontal position, that is the value of $\sigma\rho_L/G^2l$, for a vertical broken line A-A independently of ρ_G/ρ_L, and thereby the prediction of [3] is divided into two parts, H-regime and N-regime. Now, q_{co}/GH_{LG} of [2] is proportional to $(\rho_G/\rho_L)^{0.133}$ while that of [4] to $(\rho_G/\rho_L)^{0.60}$, and hence the point P appears on the r.h.s. of A-A for sufficiently high ρ_G/ρ_L ratios as shown in the upper diagram of figure 7, while the point P moves to the l.h.s. of A-A, as in the lower diagram of figure 7, if ρ_G/ρ_L reduces. Under these circumstances, it is assumed in Katto correlation that for the upper condition of figure 7, HP-regime predicted by [4] is realized starting the point P and the dotted line of [3] does not materialize, while for the lower condition of figure 7, N-regime predicted by [3] appears and the dotted lines of [2] and [4] do not materialize. In this way, when the mass velocity G is high, HP-regime can take place if the pressure (or ρ_G/ρ_L) is high, while N-regime appears if the pressure (or ρ_G/ρ_L) is low. The boundary line of the HP-possible-region shown in figure 1 has been obtained from the condition of coincidence of the horizontal position between the point P and the line A-A in figure 7, neglecting the transition zone which should exist between HP- and N-regime, for simplicity's sake.

4.2 *Classification of CHF data to characteristic regimes*

The marks (HP), (H) and (N) attached to the experimental data in figures 4–6 represent the classification of data to HP-, H- and N-regime respectively on the basis of the criteria explained in figure 7. The pressure conditions of $p = 24.5$ and 19.6 bar in figure 4, however, correspond to

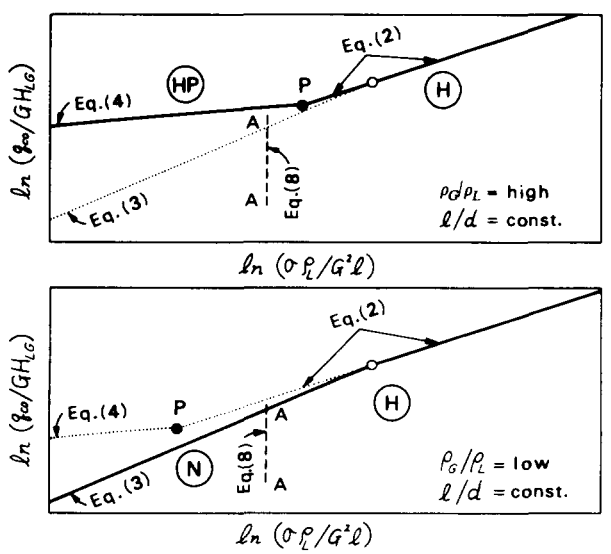

Figure 7. Criterion for the onset of HP- and N-regime.

the points C and D in figure 1. In other wards, they are in the vicinity of the boundary of the HP-possible-region. Strictly speaking, it means being in a transition zone lying between HP- and N-regime, and this is the reason why question marks are attached to (HP) at $p = 24.5$ bar and to (N) at $p = 19.6$ bar respectively.

In figure 4, the data classified to H-regime show the linear $q_c - \Delta H_i$ relationship throughout the experimental range of ΔH_i, whereas the data in N-regime deviate from the above character. These are in accord with the respective characters of H- and N-regime assumed by Katto (1978). On the other hand, the data classified to HP-regime in figures 4 and 6 have the linear $q_c - \Delta H_i$ relationship when $G < 3800\,\mathrm{kg/m^2s}$, but exhibit anomalous trends in the region on the l.h.s. of the broken curve when $G > 3800\,\mathrm{kg/m^2s}$. In a preceding paper (Katto 1978), HP-regime was assumed to have the linear $q_c - \Delta H_i$ relationship on the basis of the experimental data of Chojnowski & Wilson (1974) for $G < 1500\,\mathrm{kg/m^2s}$ as well as of the empirical correlation of Becker *et al.* (1972). According to the results of figures 4 and 6, however, it seems likely that if G is increased extraodinarily, the linear $q_c - \Delta H_i$ relationship deteriorates in the range of small ΔH_i.

4.3 *Upstream CHF*

Figure 8 shows the experimental data of CHF obtained by Waters *et al.* (1964) for water boiling at $p = 104$ bar in a heated tube 11.2 mm in diameter and 3660 mm in length, where open symbols refer to regular CHF, while solid symbols represent upstream CHF. These are nothing but the data which Collier (1972) cited in his book as the anomalous effects due to ultra high mass velocities.

The experimental condition of figure 8 ($\rho_G/\rho_L = 0.0853$ vs $l/d = 327$) is found to fall in the HP-possible-region, but is located near the boundary in figure 1, so that the situation is similar to the case of $p = 24.5$ bar in figure 4. Besides, it is noted that the experimental results in both cases of figures 8 and 4 are very similar in character, not only for the relation between q_c and ΔH_i but also for the circumstances of generating upstream CHF. In addition, the experiments of Matzner *et al.* (1965), Merilo (1977), and Merilo & Ahmad (1979), in which upstream CHF was observed at very high mass velocities, are of the same order as that of Waters *et al.* for l/d, ρ_G/ρ_L and G. All the facts mentioned above may be regarded as suggesting that the character of

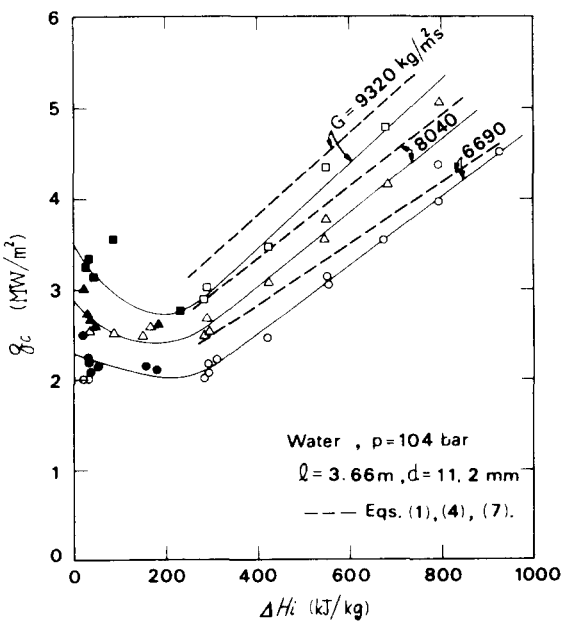

Figure 8. Experimental results of q_c for water, $\rho_G/\rho_L = 0.0853$ and $l/d = 327$ (Waters *et al.* 1964).

CHF such as shown in figure 4 is common to R-12 and water. At the present state, however, it seems premature to discuss the relation to the upstream CHF of Groeneveld (1972, 1974), because this upstream CHF is the one observed under conditions considerably far from HP-regime and for mixed inlet conditions (that is $\Delta H_i < 0$) alone.

4.4 *Regular CHF with linear $q_c - \Delta H_i$ relationship*

Experimental values for q_c and K on the r.h.s. of [1] can be determined from straight lines in the region of linear $q_c - \Delta H_i$ relationship in figures 4 and 6, and they are compared with the predictions of q_{co} and K given by [2]–[7] in figures 8–10. Physical properties used are those of the saturated condition at inlet pressure p. Presenting the data on log scale, as in figures 8–10, may not be fair as regards accuracies, but it is more important at present to seize the character of the q_{co} and K data, for which log scale is suitable.

First, in figure 9, open circles represent the measured values of q_{co} determined from the data† of figure 4, while heavy lines indicate the predicted q_{co}, for which characteristic regimes

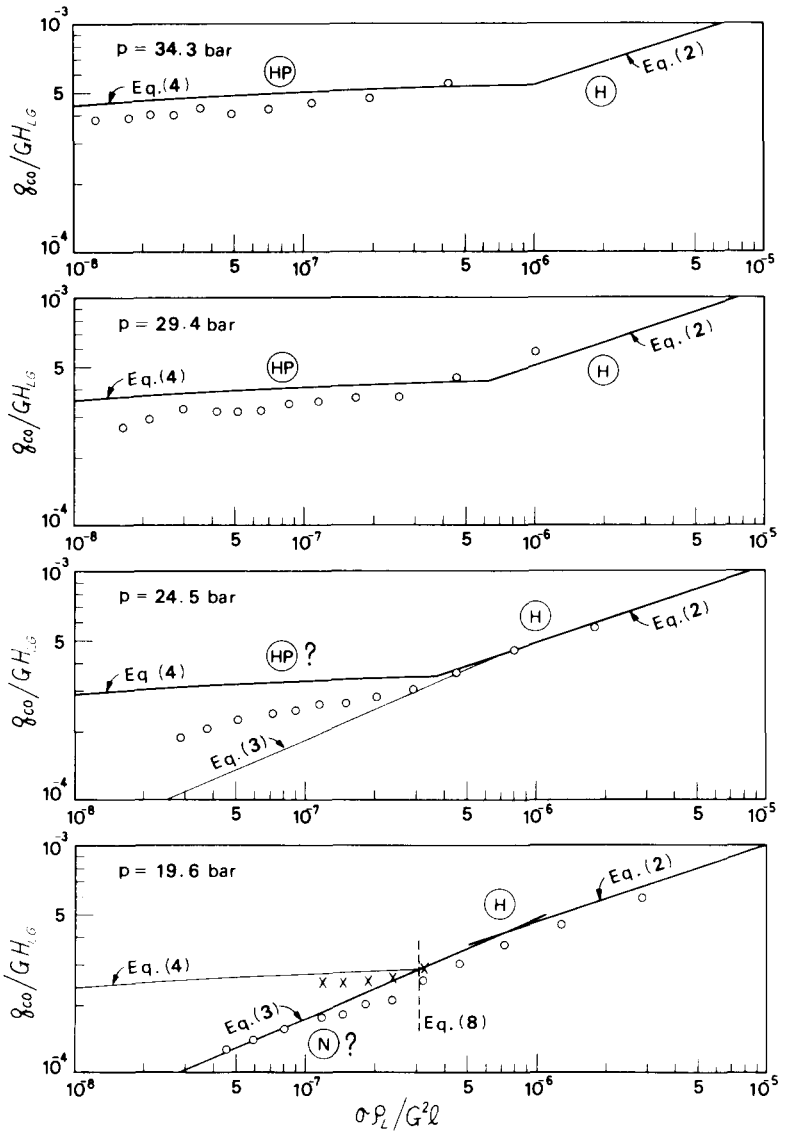

Figure 9. Comparison between the measured and the predicted q_{co} (R-12, $d = 5$ mm, and $l = 1000$ mm).

†Additional data obtained for $G = 1600$, 2700, 3800 (or 3900), and 4800 (or 4900) kg/m^{2}s, which are omitted from the presentation in figure 4 to avoid complexity, are also used.

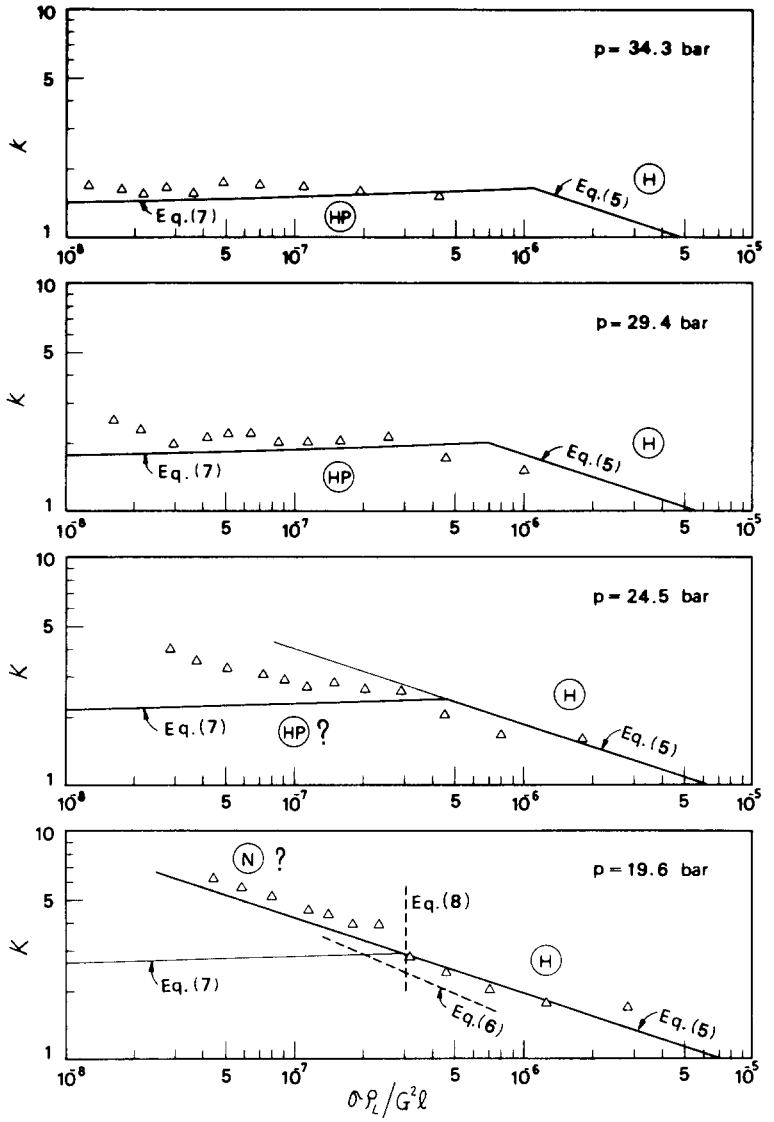

Figure 10. Comparison between the measured and the predicted K (R-12, $d = 5$ mm, and $l = 1000$ mm).

determined in figure 4 are shown with the same marks: (HP), (H), (HP) and (N). For $p = 34.3$ and 29.4 bar (points A and B in figure 1), the agreement between the measured and the predicted q_{co} is fairly well. For $p = 24.5$ bar (point C in figure 1), the measured q_{co} in the range of $\sigma\rho L/G^2l < 3 \times 10^{-7}$ lies between the predictions of [3] and [4], suggesting the trend of transition from HP-regime. Then, for $p = 19.6$ bar (point D in figure 1), the measured q_{co} in the range of $\sigma\rho_L/G^2l < 3 \times 10^{-7}$ agrees with the prediction of [3], exhibiting the clear separation from HP-regime. However, it should be noted that this does not mean the appearance of N-regime in its pure form, because the values of q_{co} determined through the extrapolation as $\Delta H_i \to 0$ of the data for $p = 19.6$ bar in figure 4 are represented by crosses in figure 8 showing a deviation from the prediction of [3] for q_{co} in N-regime.

Next, in figure 10, triangular symbols representing the experimental values of K determined from the data of figure 4 are compared with the predicted k given by [5]–[7], showing quite the same character as that of figure 9 in the relation to the characteristic regimes. It is noted in the case of $p = 19.6$ bar that the experimental data of q_{co} for $\sigma\rho_L/G^2l < 7 \times 10^{-7}$ in figure 9 agree well with the prediction of [3], whereas the corresponding data of K for $\sigma\rho_L/G^2l < 7 \times 10^{-7}$ in figure 10 are near the prediction of [5] than that of [6] which corresponds to [3]. A similar result has already been

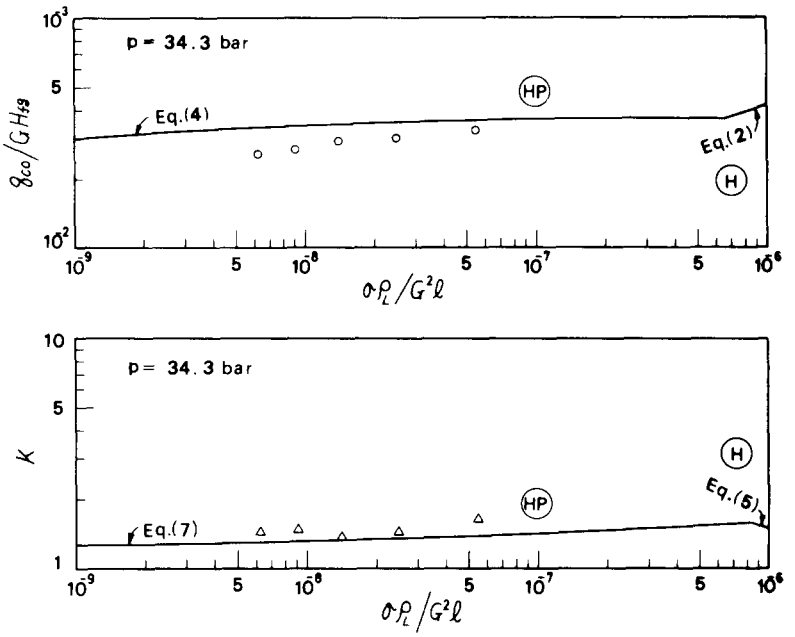

Figure 11. Comparison of the measured q_{co} and K with the predicted q_{co} and K (R-12, $d = 3$ mm, and $l = 1000$ mm).

obtained in the preceding study of one of the authors (see Section 3.1 of Katto 1980b), and hence the use of [5] instead of [6] seems preferable for predicting the approximate values of K in N-regime.

Figure 11 shows the comparison of the experimental values of q_{co} and K obtained from the result of figure 6 (point E in figure 1) with the predicted q_{co} and K. The experimental values agree fairly well with the prediction, and the general feature is similar to that in the case of $p = 34.3$ and 29.4 bar in figures 9 and 10.

Finally, three broken lines drawn in figure 8 represent the prediction of q_c calculated through [1] and the correlation equations [4] and [7] for HP-regime. They show some deviations from the experimental data, but it may be rather natural because the experimental condition of figure 8 is in a transition zone from HP-regime to N-regime as has been mentioned in Section 4.3.

4.5 *Shah generalized correlation and regular CHF data*

So far regular CHF data have been analyzed on the basis of Katto correlation. Next, the prediction of Shah correlation is compared with the regular CHF data in figure 12 in quite the same manner as in figure 9. Each curve in figure 12 represent the prediction of q_{co} derived from Shah correlation for the conditions of R-12, $d = 5$ mm, $l = 1000$ mm and $\Delta H_i = 0$, while the experimental data are the same as those in figure 9. It is noted from figure 12 that Shah prediction agrees fairly well with the data all over the experimental range of pressure from 34.3 to 19.6 bar, and particularly the agreement is satisfactory at $p = 24.5$ bar. However, a systematic difference of trend is observed in the range of low $\sigma\rho_L/G^2l$ in figure 12 that the prediction curve keeps nearly an identical form throughout the experimental range of pressure, whereas the data points line almost horizontally at high pressures ($p = 34.3$ and 29.4 bar) and they line on a slant at low pressures ($p = 19.6$ bar). As has been stated in Chapter 1, Shah correlation assumes that the lower limit of the reduced pressure to generate the high-pressure regime is 0.6, which corresponds approximately to the condition of $p = 24.5$ bar in the present case. Therefore, it may be said that Shah correlation exhibits the highest accuracy near the boundary of HP-regime, that is, near $p = 24.5$ bar, whereas Katto correlation gives the lowest accuracy there.

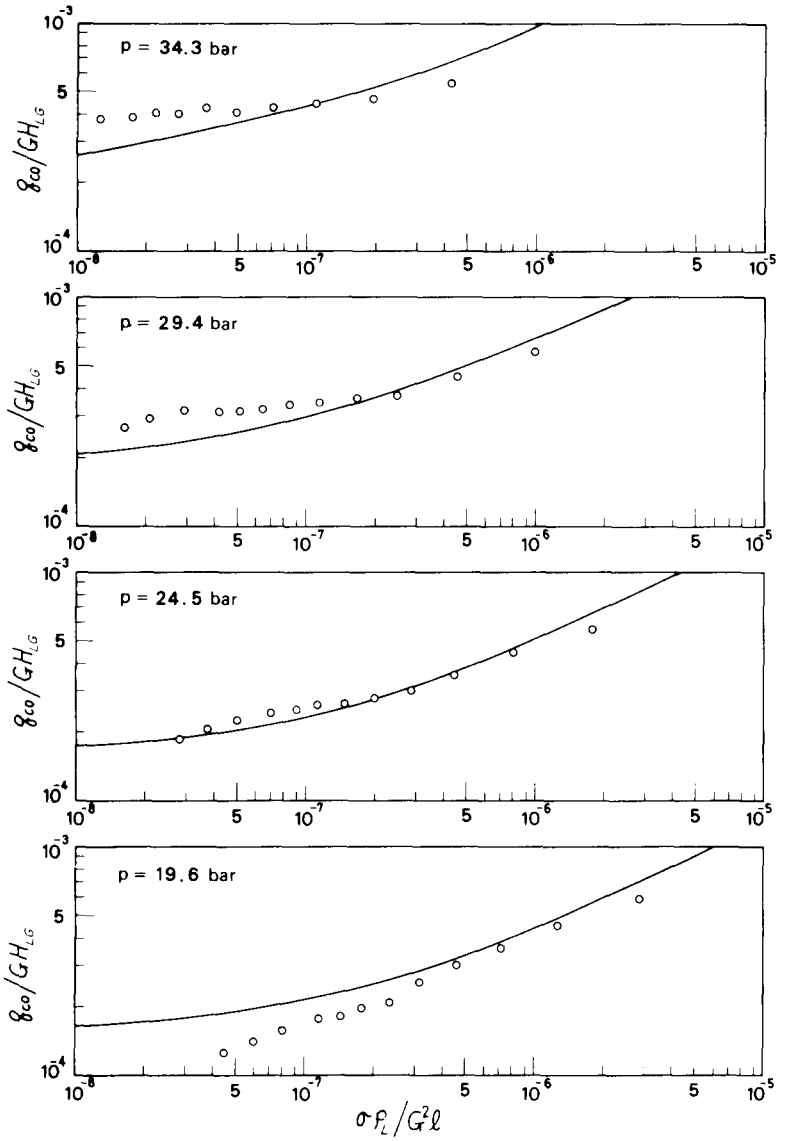

Figure 12. Comparison of the measured q_{co} with the prediction of Shah correlation (R-12, d = 5 mm, and l = 1000 mm).

4.6 *Change of physical properties due to pressure drop*

Figure 13 shows the variation of physical properties of R-12 corresponding to the pressure drop $-\Delta p$ produced over the test tube.

For Katto correlation, [4] and [7] indicate that the physical properties affecting CHF in HP-regime are H_{LG}, ρ_G/ρ_L and $\sigma\rho_L$. However, if the change of ρ_L is now neglected for simplicity's sake, they may be reduced to H_{LG}, ρ_G and σ. It is noted from figure 13 that the change of σ is exceptionally great in HP-regime (p = 34.3 and 29.4 bar). However, as is seen in figures 9–11, both q_{co} and K in HP-regime hardly change with the change of $\sigma\rho_L/G^2l$, so that the effect of σ on CHF in HP-regime may be neglected for rough purposes.

In the case of Shah correlation, CHF is affected by the physical properties c_{pL}/k_L, μ_L/μ_G, ρ_L, H_{LG} together with the reduced pressure p_r (which may be substituted by ρ_G/ρ_L), where c_{pL} is the specific heat of liquid, k_L the thermal conductivity of liquid, μ_L and μ_G the dynamic viscosity of liquid and vapor respectively. As is seen in figure 13, the change of μ_L/μ_G is significant in HP-regime, but Shah correlation seems to be constructed so as to give little effects of μ_L/μ_G on CHF in HP-regime.

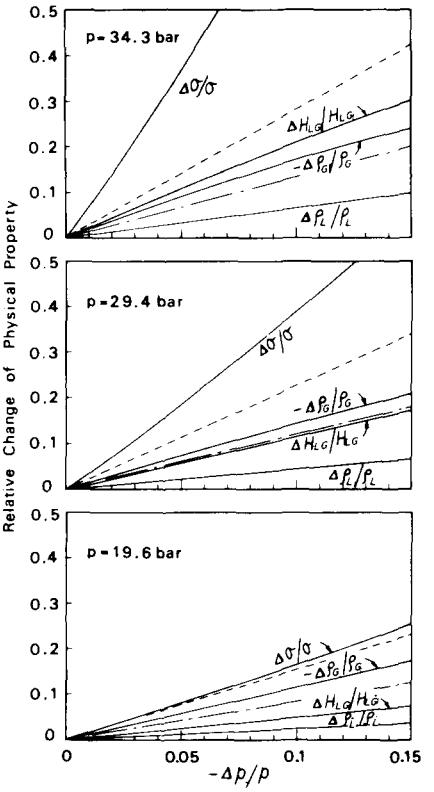

Figure 13. Change of physical properties of R-12 due to pressure drop [broken line: $\Delta(\mu_L/\mu_G)/(\mu_L/\mu_G)$, chain line: $-\Delta(c_{pL}/k_L)/(c_{pL}/k_L)$].

Now, if a limited range of mass velocity, say, $G < 3800\,\mathrm{kg/m^2s}$, is considered, then the linear $q_c - \Delta H_i$ relationship holds invariably for $\Delta H_i > 0$ (see Section 4.2), and it follows that $-\Delta p/p < 0.03 \sim 0.04$ for HP-regime in figures 5 and 6, and consequently $\Delta H_{LG}/H_{LG}$, $-\Delta\rho_G/\rho_G$, and $\Delta(c_{pL}/k_L)/(c_{pL}/k_L) < 0.1$ in figure 13. Principally, therefore, such a mass velocity range as mentioned above should be taken as the basis on which both Katto and Shah correlations of CHF in HP-regime are constructed with the assumption of constant physical properties.

4.7 *Wall temperature rise at the onset of CHF*

The circumstances to generate a lower wall-temperature excursion than the normal one at the onset of CHF have been described in Sections 3.1 and 3.2. However, if compared with the slow CHF observed by Groeneveld (1972), it seems preferable to say that the temperature rise measured in the present study is sharp rather than slow.

5. CONCLUSIONS

From the experimental study made on CHF of forced convection boiling of R-12 in uniformly heated tubes of diameter 5 and 3 mm and length 1000 mm, the following conclusions are drawn.

(1) For mass velocity G less than about $3800\,\mathrm{kg/m^2s}$, critical heat flux q_c in and near HP-regime exhibits a linear relationship to ΔH_i in the range $\Delta H_i > 0$. For $G > 3800\,\mathrm{kg/m^2s}$, the linear $q_c - \Delta H_i$ relationship holds for $\Delta H_i > k$, where k is a positive value increasing with G, while anomalous relation between q_c and ΔH_i appear for $k > \Delta H_i > 0$.

(2) Through both regions of $G < 3800\,\mathrm{kg/m^2s}$ and $G > 3800\,\mathrm{kg/m^2s}$, the CHF with linear $q_c - \Delta H_i$ relationship is always of the regular nature that the critical condition is detected first at the exit end of heated tube.

(3) The regular CHF data obtained for R-12 at points A, B, C, D and E in figure 1 agree fairly well with the prediction of Katto generalized correlation except for point C, near which the transition between HP- and N-regime is presumed to take place. Meanwhile, Shah generalized correlation exhibits a good agreement with the data throughout the experimental range of pressure, excepting some slight systematic deviations.

(4) In the case of 5-mm dia. tube, the anomalous CHF observed under conditions of $G > 3800\,\mathrm{kg/m^2s}$ and $k > \Delta H_i > 0$ is upstream CHF. When the tube diameter is reduced to 3 mm, the anomalous region reduces considerably and upstream CHF disappears.

(5) Regular CHF takes place with a sharp wall-temperature excursion, whereas upstream CHF shows a comparatively low temperature rise at the onset of CHF

Acknowledgments—The financial support given by the Minstry of Education, Science and Culture to this study [Special Project Research No. 505012 (1980)] is graetfully acknowledged. Also the authors express their appreciation to Mr. H. Inamura, Mr. N. Oshima and Mr. M. Watanabe for their assistance with the experiments.

REFERENCES

BECKER, K. M., DJURSING, D., LINDBERG, K., EKLIND, O. & ÖSTERDAHL C. 1972 Burnout conditons for round tubes at elevated pressures. *Prog. Heat Mass Transfer* **6**, 55–74.

CAMPOLUNGHI, F., CUMO, M., FERRARI, G., LEO, R. & VACCARO, G. 1974 Burn-out power in once-through tubular stem generators. *Heat Transfer* 1974 **IV**, 280–284.

CHOJNOWSKI, B & WILSON, P. W. 1974 Critical heat flux for large diameter steam generating tubes with circumferentially variable and uniform heating. *Heat Transfer* 1974 **IV**, 260–264.

COLLIER, J. G. 1972 *Convective Boiling and Condensation*, p. 259. McGraw-Hill, New York.

DOROSCHUK, V. E., LEVITAN, L. L. & LANTZMAN, F. P. 1975 Investigation into burnout in uniformly heated tubes. ASME-Paper No. 75-WA/HT-22.

GROENEVELD, D. C. 1972 The thermal behavior of a heated surface at and beyond dryout. Atomic Energy of Canada Ltd., AECL–4309.

GROENEVELD, D. C. 1974 The occurrence of upstream dryout in uniformly heated channels. *Heat Transfer* 1974 **IV**, 265–269.

GROENEVELD, D. C. & BORODIN, A. S. 1979 The occurrence of slow dryout in forced convective flow. In *Multiphase Transport* (Edited by VEZIROĞLU T. N.), Vol. 2, pp. 583–600. Hemisphere. Washington.

KATTO, Y. 1978 A generalized correlation of critical heat flux for the forced convection boiling in vertical uniformly heated round tubes. *Int. J. Heat Mass Transfer* **21**, 1527–1542.

KATTO, Y. 1979 An analysis of the effect of inlet subcooling on critical heat flux of forced convection boiling in vertical uniformly heated tubes. *Int. J. Heat Mass Transfer* **22**, 1567–1575.

KATTO, Y. 1980a Critical heat flux of forced convection boiling in uniformly heated vertical tubes (Correlation of CHF in HP-regime and determination of CHF-regime map). *Int. J. Heat Mass Transfer* **23**, 1573–1580.

KATTO, Y. 1980b Toward the systematic understanding of CHF of forced convection boiling (Case of uniformly heated round tubes). In *Heat Transfer in Energy Problems, Japan–U.S. Heat Transfer Joint Seminar.* Tokyo, pp. 53–60. Hemisphere, Washington.

LEE, D. H. 1970 Studies of heat transfer and pressure drop relevant to sub-critical once-through evaporators. IAEA–SM–130/56, Int. Atomic Energy Agency, Vienna.

LEVITAN, L. L. & LANTZMAN, F. P. 1975 Investigating burnout with flow of a stream-water mixture in a round tube. *Thermal Engng* **22**(1), 102–105.

MATZNER, B., MOECK, E. O., CASTERLINE, J. E. & WIKHAMMER, G. A. 1965 Critical heat flux in long tubes at 1000 psi with and without swirl promoters. ASME-Paper No. 65–WA/HT–30.

MERILO, M. 1977 Critical heat flux experiments in a vertical and horizontal tube with both Freon–12 and water as coolant. *Nucl. Engng Design* **44**, 1–16.

MERILO, M. & AHMAD, S. Y. 1979 Experimental study of CHF in vertical and horizontal tubes cooled by Freon–12. *Int. J. Multiphase Flow* **5**, 463–478.

PESKOV, O. L., SUBBOTIN, V. I., ZENKEVICH, B. A. & SERGEYEV, N. D. 1969 The critical heat flux for the flow of steam-water mixtures through pipes. In *Progress of Heat Transfer and Hydraulics of Two-phase Media* (Edited by Kutateladze), pp. 48–62. Pergamon Press, Oxford.

SHAH, M. M. 1979 A generalized graphical method for predicting CHF in uniformly heated vertical tubes. *Int. J. Heat Mass Transfer* **22**, 557–568.

THOMPSON, B. & MACBETH, R. V. 1964 Boiling water heat transfer burnout in uniformly heated tubes: a compilation of world data with accurate correlations. UKAEA, AEEW–R 356.

WATERS, E. D., ANDERSON, J. K., THRONE, W. L. & BATCH, J. M. 1964 Experimental observations of upstream boiling burnout. *Chem. Engng Prog. Symp. Ser.* **61**–57, 230–237.

WATSON, G. B., LEE, R. A. & WIENER, M. 1974 Critical heat flux in inclined and vertical smooth and ribbed tubes. *Heat Transfer* 1974 **IV**, 275–279.